Journal of Magnetism and Magnetic Materials 483 (2019) 21–26

Contents lists available at ScienceDirect

Journal of Magnetism and Magnetic Materials

journal homepage: www.elsevier.com/locate/jmmm

Research articles

Formation of the magnetic subsystems in antiferromagnetic NiO nanoparticles using the data of magnetic measurements in fields up to 250 kOe

S.I. Popkov[a], A.A. Krasikov[a], D.A. Velikanov[a], V.L. Kirillov[b], O.N. Martyanov[b], D.A. Balaev[a,*]

[a] Kirensky Institute of Physics, Federal Research Center "Krasnoyarsk Scientific Center, Siberian Branch, Russian Academy of Sciences", Krasnoyarsk 660036, Russia
[b] Boreskov Institute of Catalysis, Siberian Branch, Russian Academy of Sciences, Novosibirsk 630090, Russia

ABSTRACT

It is well-known that the fraction of surface atoms and the number of defects in an antiferromagnetic particle increase with a decrease in the particle size to tens of nanometers, which qualitatively changes the properties of the particle. Specifically, in antiferromagnetic nanoparticles, spins in the ferromagnetically ordered planes can partially decompensate; as a result, an antiferromagnetic particle acquires a magnetic moment. As a rule, uncompensated chemical bonds of the surface atoms significantly weaken the exchange coupling with the antiferromagnetic particle core, which can lead to the formation of an additional magnetic subsystem paramagnetic at high temperatures and spin-glass-like in the low-temperature region. The existence of several magnetic subsystems makes it difficult to interpret the magnetic properties of antiferromagnetic nanoparticles. It is shown by the example of NiO nanoparticles with an average size of 8 nm that the correct determination of the contributions of the magnetic subsystems forming in antiferromagnetic nanoparticles requires magnetic measurements in much stronger external magnetic fields than those commonly used in standard experiments (up to 60–90 kOe). An analysis of the magnetization curves obtained in pulsed magnetic fields up to 250 kOe allows one to establish the contributions of the uncompensated particle magnetic moment μ_{un}, paramagnetic subsystem, and antiferromagnetic particle core. The μ_{un} value obtained for the investigated NiO particles is consistent with the Néel model, in which $\mu_{un} \sim N^{1/2}$ (N is the number of magnetically active atoms in a particle), and thereby points out the existence of defects on the surface and in the bulk of a particle. It is demonstrated that the anomalous behavior of the high-field susceptibility dM/dH of antiferromagnetic NiO nanoparticles, which was observed by many authors, is caused by the existence of a paramagnetic subsystem, rather than by the superantiferromagnetism effect.

1. Introduction

It is well-known that nanoparticles of materials with the antiferromagnetic (AFM) order exhibit the magnetic properties atypical of the bulk systems [1,2]. The most important feature of the magnetic state of AFM nanoparticles is their uncompensated magnetic moment μ_{un} [1,2]. This moment is induced mainly by various defects, which lead to decompensation of spins in sublattices, i.e., in fact, break the AFM order. From the statistical considerations, the moment μ_{un} depends on whether the defects are localized on the surface or in the bulk of a particle. Néel showed [3] that the uncompensated moment can be estimated as

$$\mu_{un} \sim \mu \cdot N^{b}, \quad (1)$$

where N is the number of atoms in a particle, μ is the magnetic moment of an atom, and exponent b is 1/3 for surface defects, 1/2 for bulk defects, and 2/3 in the case of the odd number of planes with parallel spins in a particle. For particles with $N \sim 10^4$ and smaller, the μ_{un} value is already significant and comparable in the order of magnitude with the magnetic moment of ferrimagnetic nanoparticles with the same size [1,2]. Indeed, according to the numerous data, Eq. (1) is quite valid for nanoparticles of different AFM materials and the μ_{un} value can be hundreds of Bohr magnetons for particles several nanometers in size [1,4–16]. Certainly, this property broadens the range of application of AFM nanoparticles [17,18] and makes them an alternative to conventional ferri- and ferromagnetic nanoparticles.

The magnetic behavior of AFM nanoparticles is similar to that of ferri- and ferromagnetic ones. The uncompensated magnetic moment can be blocked (superparamagnetic state) or unblocked. These two states are separated on the temperature axis by the superparamagnetic (SP) blocking temperature T_B:

$$T_B = K_{eff} V / \ln(t/t_0)\, k_B. \quad (2)$$

Here, K_{eff} is the effective magnetic anisotropy constant, which includes the bulk magnetic anisotropy and surface effects; V is the particle volume; τ is the characteristic measurement time; τ_0 is the particle relaxation time (τ_0 is inversely proportional to the attempt frequency); and k_B is the Boltzmann constant.

* Corresponding author.
E-mail address: dabalaev@iph.krasn.ru (D.A. Balaev).

https://doi.org/10.1016/j.jmmm.2019.03.004
Received 15 January 2019; Received in revised form 18 February 2019; Accepted 2 March 2019
Available online 02 March 2019
0304-8853/

In the general case, the magnetization curves of a system of AFM nanoparticles are described by the equation

$$M(H) = M_{FM}(H) + \chi_{AF} \times H. \quad (3)$$

Here, $M_{FM}(H)$ is the contribution of the uncompensated magnetic moments hereinafter referred to as ferromagnetic (FM) subsystem and the term $\chi_{AF} \times H$ is responsible for the AFM particle sublattice cant (χ_{AF} is the AFM susceptibility). In the SP state (at $T > T_B$), the contribution of the FM subsystem is described by the classical Langevin function. In the blocked state (at $T < T_B$), the magnetization curve M(H) is the hysteretic function of the external field H. In this case, however, one should take into account the exchange coupling between the FM component and AFM core of a particle. In systems of AFM particles, the magnetic hysteresis loop often shifts upon cooling in an external field [19–29], which is caused by the exchange coupling between the FM component and AFM core. Therefore, in the blocked state in the low-temperature region ($T < T_B$), Eq. (3) is not simply a sum of two terms, i. e., the hysteretic (FM component) and linear dependences, which complicates the interpretation of the experimental data and extraction of the above-mentioned contributions.

To correctly analyze the magnetic properties of the systems of AFM particles and extract the contribution of the FM subsystem, one should choose the experimental conditions (temperature and maximum external field) that would ensure the saturation of the contribution of the FM subsystem; in this case, the M(H) dependence in the high-field region should pass to its linear portion corresponding to the second term in Eq. (3). The M(H) dependence similar to Eq. (3) was observed many times for different systems of AFM nanoparticles [1,4–14,16,20–35], but it was mentioned that its linear portion can only be observed in strong magnetic fields [9,32–35].

Another issue to be elucidated is the temperature behavior of the second term in Eq. (3). In many experiments, the $\chi_{AF}(T)$ dependence obtained from the magnetization curves decreased with temperature [4–6,8–10,12–14,20,25,31,36–38]. This is atypical of a bulk antiferromagnet (i. e., a polycrystalline antiferromagnet with the random distribution of crystallographic axes, at which the $\chi_{AF}(T)$ dependence increases with temperature). In addition, the absolute values of χ_{AF} were larger in several times than the values for a bulk AFM material [4,6,25,31,36–40]. This $\chi_{AF}(T)$ behavior was frequently attributed to the effect of superantiferromagnetism, i.e., one more effect predicted by Néel for small AFM particles [41,42]. The essence of this effect is that the surface spins of AFM nanoparticles with the even number of ferromagnetically ordered planes rotate stronger under the action of field ***H*** applied perpendicular to the easy magnetization axis than the spins of the inner planes. This can result in noticeable increase of magnetic susceptibility of small particles (the particle diameter should be no larger than several tens of ferromagnetically ordered planes) [9,35]. Besides, the extra susceptibility (or superantiferromagnetic susceptibility) can decrease with temperature [35].

However, when analyzing the magnetic properties of systems of AFM nanoparticles, we cannot ignore the presence of one more magnetic subsystem: there is a group of surface spins that may belong to neither the AFM core nor the FM subsystem. At sufficiently low temperatures, this additional subsystem can behave like a spin glass due to, e. g., frustration of the exchange couplings of surface spins [39,43–48]; at high temperatures, it behaves like an independent paramagnetic subsystem uncoupled with other subsystems [49,50]. Hence, we should add Eq. (3) with the term $M_{para}(H)$, which reflects the contribution of the paramagnetic subsystem:

$$M(H) = M_{FM}(H) + M_{para}(H) + \chi_{AF} \times H. \quad (4)$$

In view of the aforesaid, we may conclude that, when analyzing the magnetic properties of systems of AFM nanoparticles, it is necessary to take into account the contributions of all the above-mentioned magnetic subsystems and significantly broaden the range of magnetic fields in the experiments. Usually, the external field ranges between 50 and 90 kOe, due to standardization of facilities. However, an external magnetic field within this range is often insufficient to exactly separate the linear portion in the M(H) dependence. In this study, we demonstrate by the example of AFM NiO nanoparticles with an average size of ~8 nm that the use of strong pulsed magnetic fields (up to 250 kOe), along with the standard magnetic measurements, makes it possible to correctly determine the contributions of different magnetic subsystems forming in AFM nanoparticles, including the contribution of the FM and paramagnetic subsystems.

2. Experimental

2.1. Synthesis and characterization of the nanosized NiO sample

The NiO nanoparticles were synthesized by thermal decomposition of nickel oxalate $NiC_2O_4{\cdot}2H_2O$ prepared from $NiSO_4{\cdot}7H_2O$ (pure) and $(NH_4)_2C_2O_4{\cdot}H_2O$ (analytic grade) taken in the stoichiometric ratio: the 14-% $NiSO_4{\cdot}7H_2O$ solution was added with the corresponding stoichiometric amount (3.6%) of the $(NH_4)_2C_2O_4{\cdot}H_2O$ solution upon intermixing at a speed of 250 rpm for 20 min. The obtained whitish green precipitate was filtered and washed from $(NH_4)_2SO_4$ with distilled water. The decomposition process included the temperature rise to 400 °C for 40 min and 10-min exposure at this temperature.

The diffraction pattern of the sample under study was obtained on a Bruker D8 Advance X-ray diffractometer (Germany) in CuKα radiation at λ = 1.5418 Å (Fig. 1). All the diffraction peaks correspond to the NiO phase (PDF No. 047-1049). The NiO unit cell parameter coincides with a standard value (sp. gr. $Fm\bar{3}m$, a = b = c = 4.176 Å, and α = β = γ = 90°). The coherent scattering region determined from the diffraction peak broadening by Scheerer formula is 8 nm.

The electron microscopy investigations were carried out on a Hitachi HT7700 transmission electron microscope at an accelerating voltage of 100 kV. The samples were prepared using a conventional technique, specifically, deposition of NiO nanoparticles suspended in alcohol and preliminary dispersed in an ultrasonic bath onto carbon grids.

Fig. 2a shows a typical microphotograph of the investigated sample. Fig. 2b presents a size distribution histogram for nanoparticles with an average size of $< d > \approx 8.5$ nm, which is consistent with the coherent scattering region determined from the X-ray diffraction data (Fig. 1). The sample under study is hereinafter referred to as 8-nm NiO.

To obtain information about the behavior of the magnetic susceptibility of bulk nickel oxide, we sintered a sample from the tableted

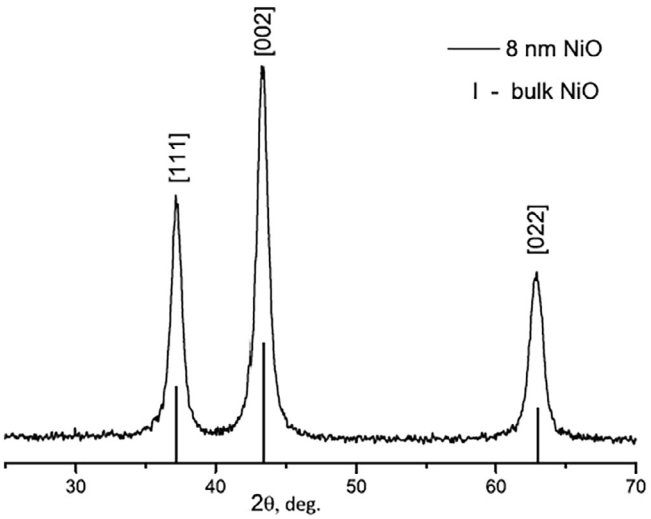

Fig. 1. Experimental diffraction pattern of the investigated NiO nanoparticle sample and line diagram showing the position and relative intensity of the bulk NiO phase peaks.

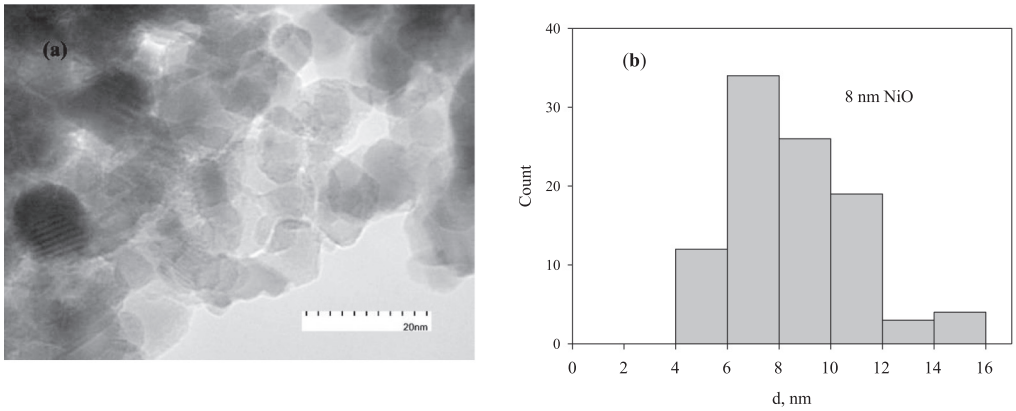

Fig. 2. Transmission electron microscopy data on the 8-nm NiO sample: (a) typical microphotograph and (b) particle size distribution histogram.

ultrahigh-purity NiO reagent at 600 °C. The measured magnetic susceptibility of the sample is denoted by $\chi_{bulk}(T)$.

2.2. Magnetic measurements in different field ranges

The temperature dependences of magnetization M(T) were obtained on a SQUID magnetometer [51] in the zero-field cooling (ZFC) and field cooling (FC) modes. The quasi-static measurements of the M(H) dependences were performed on a vibrating sample magnetometer (VSM) [52] in fields up to 60 kOe.

The measurements of the magnetization curves M(H) in pulsed magnetic fields were performed on an original pulsed magnetic field facility at the Kirensky Institute of Physics (Krasnoyarsk, Russia). The sample under study was fixed in an induction sensor placed on a measuring rod of the pulsed magnetometer. The pulse length was 16 ms. When measured in a pulsed field, a signal proportional to the magnetization is integrated during a pulse with an analog device. To eliminate the background, measurements were taken with the sample and without the sample, after which the signal from the sample determined. The magnetization isotherms M(H) were measured at temperatures of 77–300 K and a magnetic field pulse amplitude up to 250 kOe.

3. Results and discussion

3.1. Superparamagnetic blocking temperature

Fig. 3 shows temperature dependences of magnetization measured in magnetic fields of 100 and 1200 Oe in the ZFC and FC modes. The ZFC M(T) dependences have a maximum (arrows), the temperature of which shifts toward lower temperatures with increasing external field. This behavior, along with the strong effect of thermomagnetic prehistory (above ~240 K, the FC and ZFC M(T) dependences coincide), points out the SP blocking of nanoparticles in the sample under study.

The blocking temperature T_B at H = 100 Oe is about 185 K. At $\tau_0 \sim 10^{-11}$ s and $\tau_m \sim 10^1$ s (the value typical of the VSM technique [1]) and $< d > \approx 8.5$ nm ($V \sim d^3$), the blocking temperature $T_B \approx 185$ K corresponds, in accordance with Eq. (2), to a magnetic anisotropy constant of about 1.3×10^6 erg/cm^3. This exceeds the magnetic anisotropy constant of bulk nickel oxide ($K_V \approx 0.8 \times 10^5$ erg/cm^3 [48]) by an order of magnitude. Such an increase in the effective magnetic anisotropy constant K_{eff} in systems of nanoparticles is observed fairly frequently and related to the surface anisotropy, which dominates in small particles [53,44]: $K_{eff} = K_V + 6\,K_S/d$, where K_S is the surface magnetic anisotropy constant. If we take into account only the surface magnetic anisotropy, then the K_S value is ~0.15 erg/cm^2, which is typical of oxide systems [54–56]. From the other hand, interparticle magnetic interactions can result to increase of the blocking

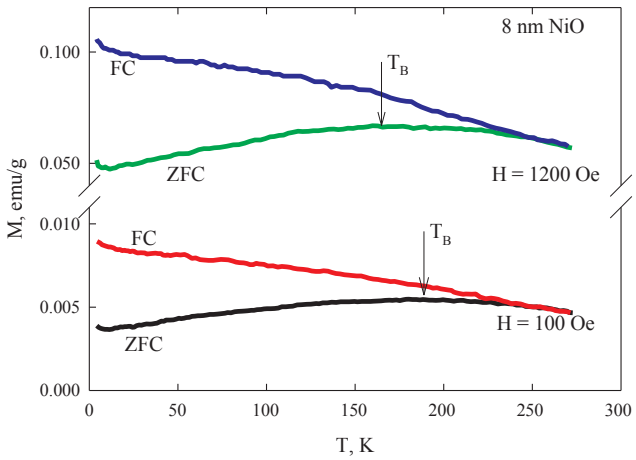

Fig. 3. Temperature dependences of magnetization for the investigated sample. Arrows show the positions of ZFC M(T) maxima (SP blocking temperature).

temperature of a system of nanoparticles (or, in seeming enhancement of the K_{eff} value) [1,16,57–63]. It should be noted that the interparticle interactions do not affect the magnetization curves in strong magnetic fields.

3.2. Magnetization isotherms in fields up to 60 kOe (VSM technique)

Fig. 4 shows M(H) dependences measured at different temperatures (below and above T_B) using the VSM technique. The curves are typical of magnetic nanoparticles: at $T < T_B$, the M(H) dependences are hysteretic (due to competition of magnetic anisotropy energy $K_{eff}V$ and Zeeman energy μ_{un}·H), while at $T > T_B$, they are fully reversible. The magnetization at 4.2 K is lower than at 78 K, which is caused by the progressive blocking of the particle magnetic moments at low temperatures. In the first approximation, the shape of the M(H) curves corresponds to the behavior predicted by Eq. (3). One can see a superposition of the field-linear contribution and FM subsystem, which exhibits the hysteresis at $T < T_B$ and is reversible at $T > T_B$. The aforementioned (see Introduction) exchange coupling between the FM component and AFM core of a particle (in fact, magnetic adherence) leads to the strong fields of the irreversible magnetization behavior and the M(H) hysteresis loops at 4.2 and 78 K in Fig. 4 are minor loops, which were observed also in other systems of AFM nanoparticles. Hence, these data do not allow us to correctly extract the contribution of the FM subsystem, since the M(H) curves do not pass to the linear portion. The data obtained in the SP temperature region do not allow us to unambiguously extract the linear M(H) portion either.

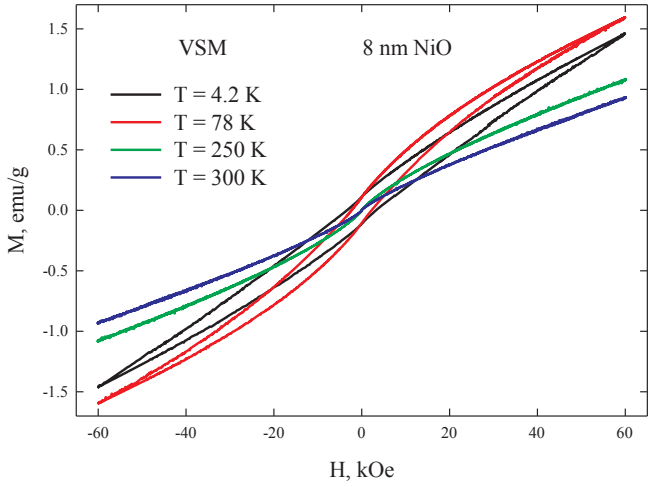

Fig. 4. Isotherms of the M(H) curves for the investigated sample obtained at different temperatures by the VSM technique.

Thus, the analysis of the magnetic measurement data obtained in the conventionally used field range faced the problems concerning the extraction of contributions of different magnetic subsystems in the system of AFM particles. The external fields up to 60 kOe are insufficient to saturate the FM subsystem.

3.3. Magnetization isotherms in fields up to 250 kOe (pulsed technique)

Fig. 5 shows M(H) dependences of the investigated sample measured at different temperatures in pulsed magnetic fields up to 250 kOe. Before analyzing the data obtained, we would like to make some comments.

The pulsed technique has certain advantages and limitations in such investigations. The advantage is the significant broadening of the external field range; the limitation is related to different characteristic measuring times τ in the pulsed technique and standard quasi-static measurement method. It is obvious that at the pulsed magnetization, the τ value will be of the same order of magnitude as the pulse length (the half-period for which the external field changes from H = 0 to its maximum value H_{max}). Substituting the value $\tau \sim 10^{-2}$ s into Eq. (2), we find that the T_B value increases by 30–50% as compared with the value ($\tau \sim 10^{1-2}$ s) for the VSM technique, which leads to an increase in the coercivity of nanoparticles upon pulsed magnetization switching [54,64–68]. This must be taken into account when analyzing the data obtained in pulsed fields.

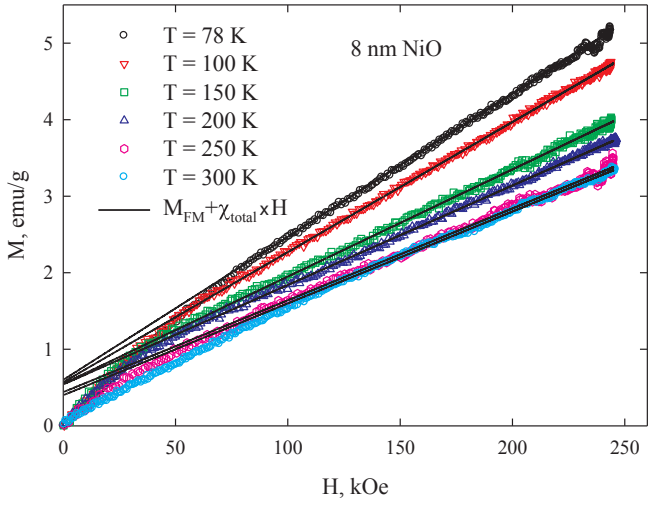

Fig. 5. Isotherms of the M(H) curves for the investigated sample. The M(H) dependences include the data obtained using a pulsed magnetometer at 0–250 kOe and the data obtained by the VSM technique in fields up to 60 kOe. Solid lines show the linear contribution extracted according to Eq. (5).

For the sample investigated in this work, a noticeable magnetization hysteresis was observed at a temperature of 78 K in fields weaker than ~130 kOe. As the temperature increases, the range of the noticeable irreversible behavior narrows: at 200 K and above, the M(H) hysteresis becomes insignificant. Fig. 5 presents the experimental M(H) dependences obtained using the VSM technique in fields below 60 kOe and the magnetization curves measured by the pulsed technique in increasing external field.

It can be seen in Fig. 5 that, in strong fields, there is a linear portion predicted by Eq. (3) under the condition that the FM subsystem is saturated (the uncompensated magnetic moments are parallel to the external field). The possible contribution of the paramagnetic subsystem (see Introduction and Eq. (4)) can be taken into account in the form $M_{para}(H,T) = M_0 B(H,T)$, where M_0 depends on the fraction of spins that exhibit the paramagnetic behavior and B(H,T) is the Brillouin function. The magnetic moment μ of the Ni^{2+} atom is ~2 μ_B; at this value, the Brillouin function is linear in field under the experimental conditions of Fig. 5 (temperatures above ~80 K and the maximum applied field is ~250 kOe). Therefore, Eq. (4) can be rewritten in the form

$$M(H, T) = M_{FM}(H, T) + \chi_{total}(T) \times H. \quad (5)$$

In this equation, $\chi_{total}(H,T)$ includes the AFM susceptibility of the particle core and the contribution of the paramagnetic subsystem: $\chi_{total}(T) = M_{para}(T)/H + \chi_{AF}(T)$. Solid lines in Fig. 5 show the approximation of the linear portion of the M(H) dependences using Eq. (5).

3.4. Uncompensated magnetic moment

The approximation of the M(H) dependences (Fig. 5) using Eq. (5) yields the $M_{FM}(T)$ values, i. e., in fact, the temperature dependence of the saturation magnetization of the FM subsystem, which is proportional to the average uncompensated magnetic moment of particles (μ_{un} in Eq. (1)) (Fig. 6). The experimental data presented in Fig. 6 are described well by the dependence

$$M_{FM}(T) = M_{FM}(T = 0) \times (1 - \beta T^{\mathbf{a}}) \quad (6)$$

at $\mathbf{a} \approx 1.75$ (± 0.1).

The temperature evolution of M_{FM} reflects the spin wave damping processes, which are different for FM and AFM materials. The situation changes with a decrease in the particle size. For example, for ferro- or ferrimagnetic nanoparticles, the exponent in Eq. (6) exceeds the value predicted by the classical spin waves theory ($\mathbf{a} = 3/2$ is the Bloch's law) [69,70]. The $\mu_{un}(T)$ behavior observed for AFM nanoparticles was also

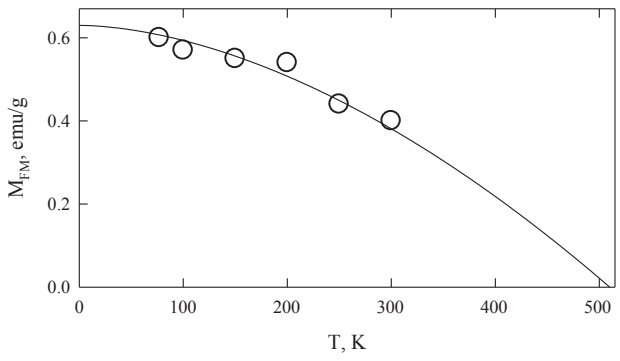

Fig. 6. Temperature dependence of M_{FM} obtained from the analysis of the data presented in Fig. 5 using Eq. (6) (dots). Approximation using Eq. (6) at $\mathbf{a} = 1.75$ (solid line).

described by functional dependence (6) [9,10,12–14]; the exponent ranged from 1.5 to 2.

The extrapolation of the data in Fig. 6 using Eq. (6) to a value of $M_{FM} = 0$ yields the temperature ~510 K. This is similar to the Néel point of the bulk NiO oxide (~520 K [71]). The temperature of magnetic ordering of nanoparticles is, as a rule, lower [71–75]. In particular, the Néel temperature of NiO particles 8 nm in size was found to be ~500 K [71].

Using the value $M_{FM}(T = 0) = 0.63$ emu/g obtained by the extrapolation of the experimental data in Fig. 6, we may determine the average uncompensated magnetic moment $< \mu_{un} >$. NiO particle with a cubic shape and mean size of $< d > \approx 8.5$ nm contains $N \sim (d/d_{Ni\text{-}Ni})^3 \approx 2.4 \times 10^4$ nickel atoms (here $d_{Ni\text{-}Ni}$ is the Ni-Ni spacing; $d_{Ni\text{-}Ni} \approx 0.3$ nm [76]). The value $M_{FM}(T = 0)$ equals to 0.63 emu/g corresponds to the decompensation of about 0.4% of nickel atoms in antiferromagnetic NiO[1]. Therefore, there are $0.004 \times N \approx 100$ nickel atoms in a particle of mean size are ordered ferromagnetically. Hence, the $< \mu_{un} >$ value for the investigated sample is ~200 μ_B. At $< \mu_{un} > \approx 200\ \mu_B$ Néel ratio (1) is valid at $b \approx 0.45$, which is similar to the case when defects exist both on the surface and in the bulk of a particle ($b = 1/2$).

3.5. Temperature behavior of the AFM susceptibility and paramagnetic subsystem

Fig. 7 presents the $\chi_{total}(T)$ dependence obtained by approximating the M(H) dependences from Fig. 5 using Eq. (5). This is, in fact, the dM(H)/dH derivative of the experimental magnetization curves in the high-field region. It can be seen that the χ_{total} value decreases with increasing temperature (see Introduction). In addition, Fig. 7 shows the temperature dependence of the AFM susceptibility for bulk NiO ($\chi_{bulk}(T)$). It can be seen that the χ_{total} values are noticeably higher than the AFM susceptibility of bulk NiO. To establish the possible contribution of the superantiferromagnetic susceptibility and (or) paramagnetic subsystem, it is necessary to subtract $\chi_{bulk}(T)$ from the $\chi_{total}(T)$ dependence. The data on the difference $\chi_{total}(T) - \chi_{bulk}(T)$ are shown in Fig. 7. It was found that the obtained values $\chi_{total}(T) - \chi_{bulk}(T)$ agree well with the dependence proportional to 1/T, i. e., are typical of the paraprocess. Thus, the excess susceptibility $\chi_{total}(T)$ is related to the existence of a paramagnetic subsystem, or from very small moments (few spins) rather than to the superantiferromagnetism.

Using the established behavior of the difference $\chi_{total}(T) - \chi_{bulk}(T)$ or, in fact, the paramagnetic susceptibility, we can determine the concentration of Ni atoms uncoupled with both the AFM particle core and FM subsystem (uncompensated moment μ_{un}). This value is about 5% of all nickel atoms in the sample[2]. For a particle with an average size of $< d > \approx 8.5$ nm, this is about 1.2×10^3 atoms, which is comparable with the number of atoms in one atomic plane ($8.5 \times 8.5\ nm^2$) or one particle face (~830 atoms). It may be said that, despite the relatively small fraction of paramagnetic atoms, their contribution to the total magnetic behavior of the sample becomes significant in strong fields. In the low-temperature region (below, at least, 80 K), it is difficult to make such estimations from the experimental M(H) curves, since the paramagnetic subsystem can exhibit the spin-glass behavior [39,43–48].

Note that, in the above estimations, we used the χ_{bulk} values for an ideal NiO particle without defects, which could induce μ_{un}, and paramagnetic atoms. However, the total number of these atoms, which are not involved in the AFM ordering, is no larger than ~6% of the total number of atoms in a particle. Therefore, the χ_{bulk} value can be assumed invariable, accurate to ~6%, for particles 8 nm in size and larger.

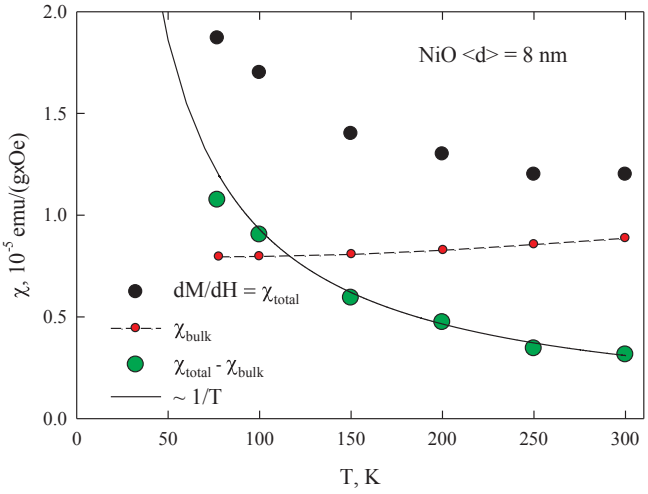

Fig. 7. The $dM/dH = \chi_{total}(T)$ values obtained by analyzing the data from Fig. 5 for the 8-nm NiO sample and temperature behavior of the AFM susceptibility of bulk NiO. The difference $\chi_{total}(T) - \chi_{bulk}(T)$ shows the temperature behavior proportional to 1/T (solid line).

4. Conclusions

The magnetic properties of nickel oxide nanoparticles with an average size of 8 nm were studied. The superparamagnetic blocking temperature for the magnetic measurements was found to be 185 K, which corresponds to the effective magnetic anisotropy constant $K_{eff} \approx 1.3 \times 10^6$ erg/cm^3. This is higher than the value for bulk nickel oxide ($\sim 0.8 \times 10^5$ erg/cm^3) by an order of magnitude and most likely caused by the surface anisotropy; the surface magnetic anisotropy constant is $K_S \approx 0.15$ erg/cm^2.

The analysis of the magnetization curves measured in the temperature range of 80–300 K and magnetic fields up to 250 kOe showed that NiO nanoparticles include three magnetic subsystems: (i) the ferromagnetic subsystem caused by the uncompensated magnetic moment of particles, (ii) antiferromagnetic subsystem of NiO nanoparticle cores, and (iii) subsystem of spins uncoupled with the antiferromagnetic core, which exhibits the paramagnetic behavior in the investigated temperature range (80–300 K). In the fields over 150 kOe, the magnetization curves pass to the linear portions due to the saturation of the ferromagnetic subsystem and field-linear response from the two other subsystems.

The temperature evolution of the high-field susceptibility (the M(H) slope in its linear portion) is described well by the two above-mentioned contributions: the inversely proportional to the temperature (paraprocess, ~1/T) and temperature dependence of the AFM susceptibility of bulk NiO. We may conclude that the observed temperature dependence of the high-field magnetic susceptibility of AFM nanoparticles is caused by a contribution arising from isolated (paramagnetic) spins or very small clusters, rather than by the superantiferromagnetism. In the investigated system of NiO nanoparticles, the fraction of the discussed paramagnetic subsystem is ~5%.

Using the data on the saturation magnetization of the system, we determined the average magnetic moment of a particle, which was found to be ~200 μ_B. This value corresponds to the decompensation of 100 nickel atoms in a particle; the Néel ratio $\mu_{un} \sim \mu \cdot N\ b$ is valid at a value of $b \approx 0.45$ similar to the idealized case ($b \approx 0.5$) of surface and bulk defects.

[1] The theoretical magnetization of NiO at $\mu_{Ni} \approx 2\ \mu_B$ for the total spin polarization is ~148 emu/g.

[2] The values $M_{para}(T)/H = \chi_{total}(T) - \chi_{AF}(T)$ in Fig. 7 are described by the expression $M_{para}(H,T) = M_0 B(H,T)$, where B(H,T) is the Brillouin function and $M_0 \approx 8$ emu/g, which corresponds to a paramagnetic atom fraction of ~(8/148) ~ 5%.

Acknowledgments

We are grateful S.V. Semenov and A.A. Dubrovskiy for their help, S.V. Komogortsev and A.D. Balaev for fruitful discussions, and M.N. Volochaev for the TEM measurements. The TEM investigations were carried out on the equipment of the Center of Collective Use of the Federal Research Center "Krasnoyarsk Scientific Center, Siberian Branch, Russian Academy of Sciences".

The reported study was funded by Russian Foundation for Basic Research, Government of Krasnoyarsk Territory, Krasnoyarsk Regional Fund of Science, to the research project: «Magnetic reversal of magnetic nanoparticles in strong pulsed magnetic fields - a new approach to the study of dynamic effects associated with the magnetization of magnetic nanoparticles» (project no. 18-42-240012).

References

[1] S. Mørup, D.E. Madsen, C. Fradsen, C.R.H. Bahl, M.F. Hansen, J. Phys.: Condens. Matter 19 (2007) 213202.
[2] Yu.L. Raikher, V.I. Stepanov, J. Phys.: Condens. Matter. 20 (2008) 204120.
[3] L. Néel, C.R. Acad, Sci. Paris 252 (1961) 4075.
[4] S.A. Makhlouf, F.T. Parker, A.E. Berkowitz, Phys. Rev. B 55 (1997) R14717.
[5] M.S. Seehra, V.S. Babu, A. Manivannan, J.W. Lynn, Phys. Rev. B 61 (2000) 3513.
[6] A. Punnoose, T. Phanthavady, M.S. Seehra, N. Shah, G.P. Huffman, Phys. Rev. B 69 (2004) 054425.
[7] N.J.O. Silva, V.S. Amaral, A. Urtizberea, R. Bustamante, A. Millan, F. Palacio, E. Kampert, U. Zeitler, S. de Brion, O. Iglesias, A. Labarta, Phys. Rev. B 84 (2011) 104427.
[8] J.G.E. Harris, J.E. Grimaldi, D.D. Awschalom, A. Chilero, D. Loss, Phys. Rev. B 60 (1999) 3513.
[9] C. Gilles, P. Bonville, H. Rakoto, J.M. Broto, K.K.W. Wong, S. Mann, J. Magn. Magn. Mater. 241 (2002) 430.
[10] N.J.O. Silva, V.S. Amaral, L.D. Carlos, Phys. Rev. B 71 (2005) 184408.
[11] A.A. Lepeshev, I.V. Karpov, A.V. Ushakov, D.A. Balaev, A.A. Krasikov, A.A. Dubrovskiy, D.A. Velikanov, M.I. Petrov, J. Supercond. Nov. Magn. 30 (2017) 931.
[12] D.A. Balaev, A.A. Dubrovskii, A.A. Krasikov, S.V. Stolyar, R.S. Iskhakov, V.P. Ladygina, E.D. Khilazheva, JETP Lett. 98 (3) (2013) 139.
[13] D.A. Balaev, A.A. Krasikov, A.A. Dubrovskii, S.V. Semenov, O.A. Bayukov, S.V. Stolyar, R.S. Iskhakov, V.P. Ladygina, L.A. Ishchenko, J. Exp. Theor. Phys. 119 (3) (2014) 479.
[14] D.A. Balaev, A.A. Krasikov, A.A. Dubrovskiy, S.I. Popkov, S.V. Stolyar, O.A. Bayukov, R.S. Iskhakov, V.P. Ladygina, R.N. Yaroslavtsev, J. Magn. Magn. Mater. 410 (2016) 71.
[15] J.T. Richardson, D.I. Yiagas, B. Turk, K. Forster, M.V. Twigg, J. Appl. Phys. 70 (1991) 6977.
[16] C.R.H. Bahl, M.F. Hansen, T. Pedersen, S. Saadi, K.H. Nielsen, B. Lebech, S. Mørup, J. Phys.: Condens. Matter 18 (2006) 4161–4175.
[17] S.V. Stolyar, D.A. Balaev, V.P. Ladygina, et al., J. Supercond. Nov. Magn. 31 (2018) 2297.
[18] K. Dobretsov, S. Stolyar, A. Lopatin, Acta Otorhinolaryngol. Ital. 35 (2) (2015) 97.
[19] H. Bi, Sh. Li, Y. Zhang, Y. Du, J. Magn. Magn. Mater. 277 (2004) 363.
[20] S.A. Makhlouf, F.T. Parker, F.E. Spada, A.E. Berkowitz, J. Appl. Phys. 81 (8) (1997) 5561.
[21] S.A. Makhlouf, H. Al-Attar, R.H. Kodama, Solid State Commun. 145 (2008) 1.
[22] M.S. Seehra, A. Punnoose, Solid State Commun. 128 (2003) 299.
[23] C. Diaz-Guerra, M. Vila, J. Piqueras, Appl. Phys. Lett. 96 (2010) 193105.
[24] A. Punnoose, M.S. Seehra, J. Appl. Phys. 91 (10) (2002) 7766.
[25] A. Punnoose, H. Magnone, M.S. Seehra, J. Bonevich, Phys. Rev. B 64 (2001) 174420.
[26] J.F.K. Cooper, A. Ionescu, R.M. Langford, K.R.A. Ziebeck, C.H.W. Barnes, R. Gruar, C. Tighe, J.A. Darr, N.T.K. Thanh, B. Ouladdiaf, J. Appl. Phys. 114 (2013) 083906.
[27] A.E. Bianchi, S.J. Stewart, R.D. Zysler, G. Punte, J. Appl. Phys. 112 (2012) 083904.
[28] D.A. Balaev, A.A. Krasikov, A.A. Dubrovskiy, S.V. Semenov, S.I. Popkov, S.V. Stolyar, R.S. Iskhakov, V.P. Ladygina, R.N. Yaroslavtsev, Phys. Solid State 58 (2) (2016) 287.
[29] D.A. Balaev, A.A. Krasikov, A.A. Dubrovskiy, S.I. Popkov, S.V. Stolyar, R.S. Iskhakov, V.P. Ladygina, R.N. Yaroslavtsev, J. Appl. Phys. 120 (2016) 183903.
[30] Ch. Rani, S.D. Tiwari, Appl. Phys. A 123 (2017) 532.
[31] S.D. Tiwari, K.P. Rajeev, Solid State Commun. 152 (2012) 1080.
[32] D.A. Balaev, A.A. Dubrovskiy, A.A. Krasikov, S.I. Popkov, A.D. Balaev, K.A. Shaikhutdinov, V.L. Kirillov, O.N. Mart'yanov, Phys. Solid State 59 (N8) (2017) 1547.
[33] D.A. Balaev, S.I. Popkov, A.A. Krasikov, A.D. Balaev, A.A. Dubrovskiy, S.V. Stolyar, R.N. Yaroslavtsev, V.P. Ladygina, R.S. Iskhakov, Phys. Solid State 59 (N 10) (2017) 1940.
[34] R.P. Guertin, N. Harrison, Z.X. Zhou, S. McCall, F. Drymiotis, J. Magn. Magn. Mater. 308 (2007) 97.
[35] N.J.O. Silva, A. Millan, F. Palacio, E. Kampert, U. Zeitler, V.S. Amaral, Phys. Rev. B 79 (2009) 104405.
[36] Ch. Rani, S.D. Tiwari, Physica B 513 (2017) 58.
[37] Ch. Rani, S.D. Tiwari, J. Magn. Magn. Mater. 385 (2015) 272.
[38] M.S. Seehra, A. Punnoose, Phys. Rev. B 64 (2001) 132410.
[39] N. Rinaldi-Montes, P. Gorria, D. Martínez-Blanco, A.B. Fuertes, L. Fernández Barquín, I. Puente-Orench, J.A. Blanco, Nanotechnology 26 (2015) 305705.
[40] M.S. Seehra, P. Dutta, H. Shim, A. Manivannan, Solid State Commun. 129 (2004) 721.
[41] L. Néel, C.R. Acad, Sci. Paris 253 (1961) 203.
[42] L. Néel, C.R. Acad, Sci. Paris 253 (1961) 1286.
[43] R.H. Kodama, A.E. Berkowitz, Phys. Rev. B 59 (1999) 6321.
[44] E. Winkler, R.D. Zysler, M. Vasquez Mansilla, D. Fiorani, Phys. Rev. B 72 (2005) 132409.
[45] M. Marin Tadić, D. Panjan, I. Marković, V. Spasojević Milošević, J. Alloys Compd. 509 (2011) 7134.
[46] D. Nikolić, M. Panjan, G.R. Blake, M. Tadić, J. Eur. Ceram. Soc. 35 (2015) 3843.
[47] A.A. Dubrovskiy, D.A. Balaev, K.A. Shaykhutdinov, O.A. Bayukov, O.N. Pletnev, S.S. Yakushkin, G.M. Bukhtiyarova, O.N. Martyanov, J. Appl. Phys. 118 (2015) 213901.
[48] M. Tadic, D. Nikolic, M. Panjan, G.R. Blake, J. Alloys Compd. 647 (2015) 1061.
[49] D.A. Balaev, A.A. Dubrovskiy, K.A. Shaykhutdinov, O.A. Bayukov, S.S. Yakushkin, G.A. Bukhtiyarova, O.N. Martyanov, J. Appl. Phys. 114 (2013) 163911.
[50] Yu.A. Koksharov, S.P. Gubin, I.D. Kosobudsky, G.Yu. Yurkov, D.A. Pankratov, L.A. Ponomarenko, M.G. Mikheev, M. Beltran, Y. Khodorkovsky, A.M. Tishin, Phys. Rev. B 63 (2000) 012407.
[51] D.A. Velikanov, RF Patent No. 2481591C1, Byull. Izobret. No. 13 (2013). http://www.fips.ru/Archive/PAT/2013FULL/2013.05.10/DOC/RUNWC1/000/000/002/481/591/DOCUMENT.PDF.
[52] A.D. Balaev, Yu.V. Boyarshinov, M.M. Karpenko, B.P. Khrustalev, Prib. Tekh. Eksp. 3 (1985) 167.
[53] F. Bødker, S. Mørup, S. Linderoth, Phys. Rev. Lett. 72 (1994) 282.
[54] D.A. Balaev, I.S. Poperechny, A.A. Krasikov, K.A. Shaikhutdinov, A.A. Dubrovskiy, S.I. Popkov, A.D. Balaev, S.S. Yakushkin, G.A. Bukhtiyarova, O.N. Martyanov, Yu.L. Raikher, J. Appl. Phys. 117 (2015) 063908.
[55] M.P. Proenca, C.T. Sousa, A.M. Pereira, P.B. Tavares, J. Ventura, M. Vazquez, J.P. Araujo, Phys. Chem. Chem. Phys. 13 (2011) 9561.
[56] YuV. Knyazev, D.A. Balaev, V.L. Kirillov, O.A. Bayukov, O.N. Mart'yanov, JETP Lett. 108 (8) (2018) 527.
[57] M. Knobel, W.C. Nunes, H. Winnischofer, T.C.R. Rocha, L.M. Socolovsky, C.L. Mayorga, D. Zanchet, J. Non Cryst. Solids 353 (2007) 743.
[58] W.C. Nunes, L.M. Socolovsky, J.C. Denardin, F. Cebollada, A.L. Brandl, M. Knobel, Phys. Rev. B 72 (2005) 212413.
[59] D.A. Balaev, S.V. Semenov, A.A. Dubrovskiy, S.S. Yakushkin, V.L. Kirillov, O.N. Martyanov, J. Magn. Magn. Mater. 440 (2017) 199.
[60] H. Shim, P. Dutta, M.S. Seehra, J. Bonevich, Solid State Commun. 145 (2008) 192.
[61] T.S. Berquó, J.J. Erbs, A. Lindquist, R.L. Penn, S.K. Banerjee, J. Phys.: Condens. Matter 21 (2009) 176005.
[62] M. Tadic, S. Kralj, M. Jagodic, D. Hanzel, D. Makovec, Appl. Surf. Sci. 322 (2014) 255.
[63] M. Tadic, S. Kralj, Y. Lalatonne, L. Motte, Appl. Surf. Sci. 476 (2019) 641.
[64] I.S. Poperechny, Yu.L. Raikher, V.I. Stepanov, Phys. Rev. B 82 (2010) 174423.
[65] I.S. Poperechny, Yu.L. Raikher, Physica B 435 (2014) 58–61.
[66] Yu.P. Kalmykov, B. Ouari, S.V. Titov, J. Appl. Phys. 120 (2016) 053901.
[67] D.A. Balaev, A.A. Krasikov, A.A. Dubrovskii, A.D. Balaev, S.I. Popkov, V.L. Kirillov, O.N. Martyanov, J. Supercond. Nov. Magn. (2018), https://doi.org/10.1007/s10948-018-4726-4.
[68] D.A. Balaev, A.A. Krasikov, D.A. Velikanov, S.I. Popkov, N.V. Dubynin, S.V. Stolyar, V.P. Ladygina, R.N. Yaroslavtsev, Phys. Solid State 60 (10) (2018) 1973.
[69] J.P. Chen, C.M. Sorensen, K.J. Klabunde, G.C. Hadjipanayis, E. Devlin, A. Kostikas, Phys. Rev. B 54 (13) (1996) 9288.
[70] C. Martínez-Boubeta, K. Simeonidis, M. Angelakeris, N. Pazos-Pérez, M. Giersig, A. Delimitis, L. Nalbandian, V. Alexandrakis, D. Niarchos, Phys. Rev. B 74 (2006) 054430.
[71] S. Thota, J.H. Shim, M.S. Seehra, J. Appl. Phys. 114 (2013) 214307.
[72] J. Wang, W. Wu, F. Zhao, G. Zhao, J. Appl. Phys. 109 (2011) 056101.
[73] X.G. Zheng, C.N. Xu, K. Nishikubo, K. Nishiyama, W. Higemoto, W.J. Moon, E. Tanaka, E.S. Otabe, Phys. Rev. B 72 (2005) 014464.
[74] A.E. Bianchi, S.J. Stewart, R.D. Zysler, G. Punte, J. Appl. Phys. 112 (2012) 083904.
[75] YuA. Kumzerov, N.F. Kartenko, L.S. Parfen'eva, I.A. Smirnov, A.A. Sysoeva, H. Misiorek, A. Jezowski, Phys. Solid State 54 (2012) 1066.
[76] W.-L. Jang, Y.-M. Lu, W.-S. Hwang, T.-Li Hsiung, H.P. Wang, Appl. Phys. Lett. 94 (2009) 062103.